

**Parametric study of particle sedimentation by dissipative particle dynamics simulation**

Lingqi Yang and Huiming Yin\*

*Columbia University, 500 West 120th Street, New York, New York 10027, USA*

(Received 4 February 2014; revised manuscript received 21 August 2014; published 24 September 2014)

A parametric study on the simulation of a single aluminum (Al) particle settling in water is conducted using various sets of interactive parameters between Al and water particles, so that a systematic method can be established to describe the hydrodynamic interaction between an Al particle and the fluid in a large range of particle sizes. The force parameters and the cutoff have been correlated to the terminal settling velocity of the Al particle in the dissipative particle dynamics simulation, so that the classic Stokes' law can be used to determine those parameters. Two empirical equations are developed to calculate the minimum repulsive force parameter in terms of the number density and radius, respectively. In addition, the correlation between the cutoff and the Al particle radius has been obtained by linear curve fitting. The radial distribution functions of Al and water particles are computed to examine the relative spacing among solid and fluid particles. The present approach is general and can also be extended to study particle motion of other types of particles and fluids. This study will be a baseline for the investigation of multiple particles settling in a viscous fluid.

DOI: [10.1103/PhysRevE.90.033311](https://doi.org/10.1103/PhysRevE.90.033311)

PACS number(s): 47.11.-j, 47.61.-k

**I. INTRODUCTION**

Traditional macroscopic description, such as Navier-Stokes equation, has been widely used to solve most engineering fluid problems [1]. Due to the increasing needs to investigate the physics of fluids at a fine scale, molecular dynamics (MD) simulation, which basically solves equations of motion of atoms, has been developed in the past decades. However, the time and length scales in the MD are so small that it is only limited to some specific problems and has been hardly used in actual engineering problems in the mesoscopic or continuum level [2]. On the other hand, the dissipative particle dynamics (DPD), as one of the thriving mesoscopic methods, is developed to bridge the gap between the continuum and atomistic level for simulating complex fluids [3]. Due to its natural soft potential, it becomes a very promising tool to describe the hydrodynamic behavior at a mesoscale level [4].

DPD was firstly introduced by Hoogerbrugge and Koelman [5,6]. Instead of defining a potential directly as classic MD potential, DPD defines three types of pairwise interaction forces between particles, namely a conservative force  $f_c$ , a dissipative force  $f_d$ , and a random force  $f_r$ , which are limited to particles within the cutoff distance  $r_{cut}$ . Each force has a force parameter to tune its magnitude and a certain relation between the dissipative and the random force parameters has to be satisfied so that a correct thermostat can be obtained as a canonical ensemble. In a DPD system, a single DPD particle, which is actually a mathematical point in the simulation, stands for a cluster of real molecules or a physical particle. Therefore, DPD can also be considered as a coarse-grained MD method in which a coarse-graining parameter ( $N_m$ ) is normally used to characterize the number of molecules represented by the particle. Because of its capability to describe the hydrodynamic behavior, it has been applied to study various

problems involving colloidal suspension [7–9], polymers [10–12], and multiphase flow [13,14].

A milestone work by Groot and Warren [3] has critically reviewed the DPD method and established several useful guidelines for choosing DPD force parameters. By matching the dimensionless compressibility of water at room temperature, an analytical form is derived for the repulsive force parameter of water-water particles when one water particle only represents one water molecule ( $N_m = 1$ ). Several other interesting results have also been discussed by the authors, such as the viscosity, multiphase, etc. Such a systematic study has provided the foundation for researchers to refine its force terms to set up their DPD simulation compatible with more complicated hydrodynamic behavior, such as the satisfaction of the no-slip boundary conditions in DPD [15–18] and liquid-vapor interface [19–21] by many-body DPD (MDPD).

Even though DPD has shown its unique advantages on describing hydrodynamic behavior from the mesoscopic level, it has its inherent drawbacks in describing fluid transport properties and relation between the DPD scale and the real physical scale. Several studies have comprehensively investigated the effect from the dissipative and random force parameters [3,5,13,22,23], different integration schemes [3,24–26], Lowe-Andersen thermostat [23,27,28], and the scaling and mapping procedures [29–32], which determine the transport properties, such as diffusion coefficient, Schmidt number ( $Sc$ ), viscosity, etc. in a DPD fluid. It has been pointed out [3,28,30,33,34] that the  $Sc$  in DPD is normally three orders of magnitude smaller than the real fluid and such discrepancy increases as  $N_m$  increases. Such coarse graining issues can be explained by rigorous mathematical derivations, showing that the coarse-grained dynamics is actually a non-Markovian process, which could make DPD impractical [35,36]. Numerous efforts have been made to reduce the gap between DPD and real fluids. For example, a larger dissipative force parameter could be used to obtain a correct  $Sc$  number, while the timestep should be reduced correspondingly in order to maintain the system temperature control, it however leads to the loss of the time scaling advantage. Therefore, most existing

\*yin@civil.columbia.edu

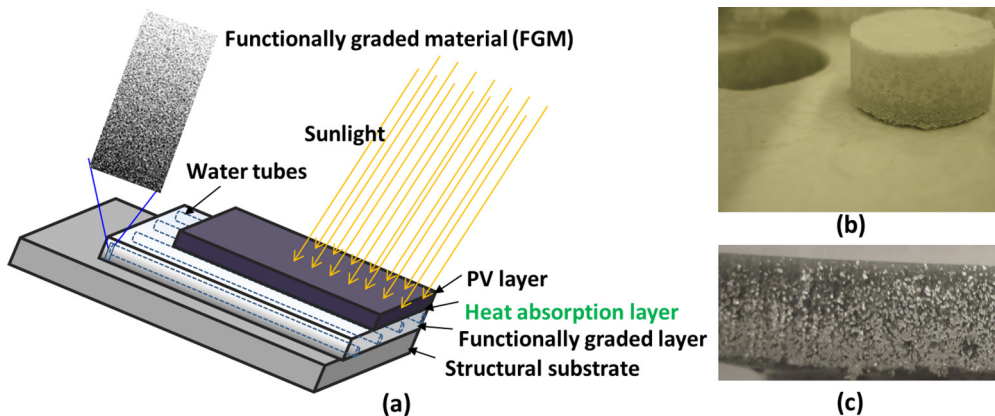


FIG. 1. (Color online) Sedimentation-based manufacturing of a functionally graded material for a hybrid solar roofing panel. (a) Schematic illustration of the roofing panel; (b) a graded mix of Al and HDPE particles produced by sedimentation; and (c) a functionally graded material obtained by sintering the graded mix.

studies have adopted the numerical value of the dissipative force parameters recommended by Groot and Warren [3], so that the system can maintain the temperature control at a relative reasonable timestep while a targeted hydrodynamic behavior can still be achieved while missing some physical properties.

Another drawback of DPD is that it is not straightforward to establish the direct correlation between the DPD scale and the physical scale, because problems are normally solved by DPD in reduced units, and lack of rigorous derivation of DPD force parameters limits work in quantitatively describing a practical engineering problem. Kumar [30] provided a detailed explanation on mapping the DPD scale to the real physical scale via the coarse-grained parameter ( $N_m$ ). Similar units mapping procedure can be found in several other articles [37–41]. By state of the art in DPD, calibration and validation of DPD force parameters are still very challenging. One common approach among the existing literature is to match the desired properties with the experimental values, like dimensionless compressibility [3,28,33], diffusion constant [37] and viscosity [30] of liquid, unique material structure [38,42], or mechanical behaviors [41,43]. However, for a realistic multicomponent system, there is still no systematic methodology to define the interaction forces between the solute and solvent particles. For example, in most of the DPD simulation of polymer suspension, a simple DPD fluid particle is commonly used to replace the bead in a bead-spring model for polymer [11,44,45]. Similar magnitudes of the repulsive force parameter as the one from Groot and Warren's work [3] are applied for bead-bead, bead-solution, and solution-solution particles' interaction. Maiti and McGrother [10] have revised the polymer model by presenting a thorough analysis on scaling the DPD force parameters with the bead size by matching the computed surface tension of segregated components with the experimental interfacial tension. Following this numerical procedure, one can similarly extend this work to more complex mixture systems. For colloidal suspension, using a certain number of local freezing fluid particles to form a big cluster, the rough sphere model, has been proposed to provide a good agreement with the continuum fluid mechanics [7,46,47].

However, the inflexibility in its geometry makes it very hard to simulate a large-scale system or interaction between multiple types of particles. There are also some modifications on the DPD force terms [9,48], where the authors used an exponential conservative force for the colloid-colloid and colloid-fluid interactions.

The purpose of this paper is to establish a simple but efficient DPD model to simulate the sedimentation of a single particle with a varying diameter falling in a fluid due to the gravity, where the solid particle is represented by single DPD bead with larger repulsive force parameter and size-based cutoff. This work is motivated by the recent invention of a hybrid solar roofing panel, as in Fig. 1 [49–51]. A functionally graded material (FGM) layer made of aluminum and high density polyethylene (HDPE) is to create a light-weight layer of solar roofing panel with a varying thermal conductivity in the thickness direction, which is gradually transitioned from a well-conductive side attached with a PV solar cell (laminated by a protective layer) to another highly insulative side bonded to a structural substrate. The water flow through the FGM layer cools down photovoltaic (PV) cells and harvests the solar heat. In the manufacturing of the FGM, Al and HDPE powders are first mixed in a fluid. Due to the different densities and sizes of particles, the powders fall down to the bottom of the container at different velocities and thus form a graded microstructure. After draining out the fluid, one can obtain the functionally graded powder mix, as in Fig. 1(b). Sintering the mix, we can obtain a functionally graded composite, as in Fig. 1(c) [52–54].

To understand the sedimentation behavior of many particles, this paper first uses conventional DPD force terms to study the sedimentation of a single Al particle in water. The primary goal of this paper is to understand the size effect of the Al particle on the DPD simulation and thus set up a baseline for future simulation of many particles. The terminal settling velocity of an Al particle will be matched to the Stokes' law by scaling the repulsive force parameter and the cut-off between the Al and water particles. Based on this fundamental study, we aim to build an extended DPD model for many particles with different sizes and densities falling in a liquid.

## II. METHODOLOGY

### A. DPD theory

As a discrete particle method, DPD inherits the same algorithm as MD, which is based on Newton's second law:

$$m^I \frac{d^2 \mathbf{r}^I}{dt^2} = \mathbf{f}^I, \quad (1)$$

where  $m^I$ ,  $\mathbf{r}^I$ ,  $t$ , and  $\mathbf{f}^I$  denote mass, position vector, time, and force vectors, respectively, of particle with index  $I$ .

The conventional DPD method contains three forces between two particles acting along the line of particle centers:  $\mathbf{f}_C$ , denotes the conservative force;  $\mathbf{f}_D$ , the dissipative force; and  $\mathbf{f}_R$ , the random force. Then the total force exerted on particle  $I$  from all other particles, say particle  $J$ , within a certain cutoff  $r_{\text{cut}}$  can be written as

$$\mathbf{f}^I = \sum_{J \neq I} (\mathbf{f}_C^{IJ} + \mathbf{f}_D^{IJ} + \mathbf{f}_R^{IJ}). \quad (2)$$

The conservative force is expressed as

$$\mathbf{f}_C^{IJ} = a^{IJ} \omega_C \mathbf{n}^{IJ}, \quad (3)$$

where the weight function  $\omega_C$  is normally assumed to be a linear relation with respect to  $r^{IJ}$  ( $r^{IJ} = \mathbf{r}^I - \mathbf{r}^J$ ,  $r^{IJ} = |\mathbf{r}^{IJ}|$ ,  $\mathbf{n}^{IJ} = \mathbf{r}^{IJ}/r^{IJ}$ )

$$\omega_C = \begin{cases} 1 - \frac{r^{IJ}}{r_{\text{cut}}} & (r^{IJ} < r_{\text{cut}}), \\ 0 & (r^{IJ} \geq r_{\text{cut}}), \end{cases} \quad (4)$$

so that a soft repulsion between particles makes DPD capable for solving mesoscale problems; and  $a^{IJ}$ , the so-called repulsive force parameter, determines the maximum repulsion between two particles, which actually reflects the type of particle used in the simulation. For example, Groot and Warren [3] have successfully derived the expression for the repulsive force parameter for water-water particles in terms of the number density of DPD fluid ( $n_{\text{DPD}}$ ). The general form is given as

$$a^{\text{Water-Water}} = \frac{75k_B T}{n_{\text{DPD}}}, \quad (5)$$

where  $k_B T$  is the energy reference in reduced units, which will be elaborated in the next section. Note that Eq. (5) is only valid when  $N_m = 1$ , which implies that one DPD particle represents one single water molecule.

The dissipative force, which relates to the relative velocity vector  $\mathbf{v}^{IJ} = \mathbf{v}^I - \mathbf{v}^J$ , is given by

$$\mathbf{f}_D^{IJ} = -\gamma \omega_D (\mathbf{n}^{IJ} \cdot \mathbf{v}^{IJ}) \mathbf{n}^{IJ}, \quad (6)$$

where  $\gamma$  is the dissipative force parameter. By monitoring the temperature noise amplitude, Groot and Warren [3] have also suggested to choose  $\gamma$  as a fixed constant so that a reasonable timestep can be chosen as without losing the time-scaling advantage. Via the kinematic theory [22], a relation is found between viscosity of a DPD fluid and  $\gamma$  in the absence of the conservative force, and more generous forms are provided for the self-diffusion coefficient  $D$ , kinematic viscosity  $\nu_{\text{DPD}}$ , and the dynamic viscosity  $\mu_{\text{DPD}}$ , which are given by Refs. [3,13,23]

as follows:

$$D \approx \frac{45k_B T}{2\pi\gamma n_{\text{DPD}}(r_{\text{cut}})^3}, \quad (7)$$

$$\nu_{\text{DPD}} \approx \frac{D}{2} + \frac{2\pi\gamma n_{\text{DPD}}(r_{\text{cut}})^5}{1575}, \quad (8)$$

and

$$\mu_{\text{DPD}} = \nu_{\text{DPD}} n_{\text{DPD}}. \quad (9)$$

Because the dissipative force  $\mathbf{f}_D$  will cool down the system, the random force, which is called the stochastic force, is employed to compensate the loss of number of degrees of freedom due to the increasing scale from the molecule level to maintain a Brownian motion as

$$\mathbf{f}_R^{IJ} = \sigma \omega_R \zeta^{IJ} (\Delta t)^{-1/2} \mathbf{n}^{IJ}, \quad (10)$$

where  $\zeta^{IJ}$  is the random number with zero mean and unit variance of Gaussian distribution. According to Español and Warren [55], the weight functions  $\omega_D$  and  $\omega_R$  can be chosen arbitrarily. However, the dissipative force parameter  $\gamma$  and random force parameter  $\sigma$  have to satisfy the fluctuation dissipation theorem to act as a thermostat to control the system temperature [55]. In summary,

$$\begin{aligned} \sigma^2 &= 2\gamma k_B T \\ \omega_D &= (\omega_R)^2. \end{aligned} \quad (11)$$

A common choice for those two weight functions [3] is given as

$$\omega_D(r^{IJ}) = [\omega_R(r^{IJ})]^2 = \begin{cases} (1 - \frac{r^{IJ}}{r_{\text{cut}}})^2 & (r^{IJ} < r_{\text{cut}}), \\ 0 & (r^{IJ} \geq r_{\text{cut}}), \end{cases} \quad (12)$$

which will be used in this paper.

### B. Mapping from the DPD scale to the real physical scale

As mentioned before, problems are normally solved in reduced units in DPD. To distinguish from the one in DPD units, in this paper the variables in the physical scale use an overbar on the corresponding symbols. In order to establish the units mapping guideline, one needs to define reference units first. In general, DPD uses the cutoff radius  $\bar{r}_{\text{cut}}$  as the reference length, mass of single DPD particle  $\bar{m}_{\text{DPD}}$  as the reference mass, and  $\bar{k}_B \bar{T}_{\text{ref}}$  as the reference energy, where  $\bar{k}_B = 1.381 \times 10^{-23}$  J/K is the Boltzmann constant, and  $\bar{T}_{\text{ref}}$  is the reference temperature in Kelvin. Therefore, in the DPD unit,  $k_B T = 1.0$ . In order to simulate a practical engineering problem, Kumar [30] used the coarse-grained parameter  $N_m$  to bridge the DPD and physical scales by matching the density of the DPD fluid to the real liquid in a unit cube. Since this paper will mainly focus on water, we have the mass equivalence as

$$\bar{\rho}^{\text{Water}} \bar{r}_{\text{cut}}^3 = n_{\text{DPD}} \bar{m}_{\text{DPD}}, \quad (13)$$

where  $\bar{m}_{\text{DPD}} = N_m \times \bar{m}^{\text{Water}}$ , indicating that one DPD particle is actually a cluster with  $N_m$  water molecules. Therefore,

TABLE I. Example of units mapping from the physical scale to the DPD scale.

Input	Description	Derived	Description
$n_{\text{DPD}} = 4.0$	Number density	$N_m = 8.357 \times 10^9$	Coarse-grained param.
$\bar{r}_{\text{ref}} = 1.0 \times 10^{-6} \text{ m}$	Length reference	$\bar{m}_{\text{ref}} = 2.500 \times 10^{-16} \text{ kg}$	Mass reference
$\bar{T}_{\text{ref}} = 300 \text{ K}$	Temperature reference	$\bar{v}_{\text{ref}} = 4.070 \times 10^{-3} \text{ m/s}$	Velocity reference
		$\bar{t}_{\text{ref}} = 2.457 \times 10^{-4} \text{ s}$	Time reference
		$\bar{e}_{\text{ref}} = 4.142 \times 10^{-21} \text{ J}$	Energy reference
In the physical scale		In the DPD scale	
$\bar{g} = 9.81 \text{ m/s}^2$		$g = 0.592$	Gravity
$\Delta \bar{t} = 1.229 \mu\text{s}$		$\Delta t = 0.005$	Timestep
$\bar{k}_B \bar{T}_{\text{ref}} = 4.142 \times 10^{-21} \text{ J}$		$k_B T = 1.000$	
$\bar{\rho}^{\text{Water}} = 10^3 \text{ kg/m}^3$		$n_{\text{DPD}} = 4$	Density of water
$\bar{\rho}^{\text{Al}} = 2.699 \times 10^3 \text{ kg/m}^3$		$\rho^{\text{Al}} = 10.796$	Density of Al particle
$\bar{r}^{\text{Al}} = 0.5 \mu\text{m}$		$r^{\text{Al}} = 0.500$	Radius of Al particle
$\bar{m}^{\text{Al}} = 1.413 \times 10^{-15}$		$m^{\text{Al}} = 5.653$	Mass of Al particle

one obtains

$$\begin{aligned} \bar{r}_{\text{ref}} = \bar{r}_{\text{cut}} &= \left( \frac{n_{\text{DPD}} N_m \bar{m}^{\text{Water}}}{\bar{\rho}^{\text{Water}}} \right)^{1/3} \\ &= 3.104 \times 10^{-10} (n_{\text{DPD}} N_m)^{1/3} \text{ m} \end{aligned} \quad (14)$$

or

$$N_m = \frac{\bar{\rho}^{\text{Water}} \bar{r}_{\text{ref}}^3}{\bar{m}^{\text{Water}} n_{\text{DPD}}} = 3.343 \times 10^{28} \left( \frac{\bar{r}_{\text{ref}}^3}{n_{\text{DPD}}} \right), \quad (15)$$

where  $n_{\text{DPD}}$  ( $n_{\text{DPD}} = \rho^{\text{Water}}$  in this study) defines the number density in a unit cube with a side length  $\bar{r}_{\text{ref}}$ ;  $\bar{r}_{\text{ref}}$  is the reference length, and the mass of a single water molecule can be easily calculated as  $\bar{m}^{\text{Water}} = 2.992 \times 10^{-26} \text{ kg}$  as the reference mass.

From the above two equations, it can be seen that either  $N_m$  or  $\bar{r}_{\text{cut}}$  can be the input to initiate the units mapping process. To match the dimensionless compressibility of real liquid, the general expression of  $a^{\text{Water-Water}}$  increases linearly with  $N_m$  [28,33] with the initial value provided in Eq. (5) for  $N_m = 1$ . However, when  $N_m$  is large, say  $N_m > 20$ , the corresponding value of  $a^{\text{Water-Water}}$  leads to system solidification and it is not able to simulate the flow behavior [28]. In this paper,  $N_m$  is in the order of  $10^9$  at the mesoscale. To maintain the mobility of water particles, following the literature [30,56], Eq. (5) is still used. Under this condition, the dimensionless compressibility of the fluid is orders of magnitude smaller than the actual value, while the density of water is still matched at this scale from Eq. (13) to successfully simulate the flow behavior.

The mass reference in DPD will use the mass of single DPD particle, which is given by

$$\bar{m}_{\text{ref}} = \bar{m}_{\text{DPD}} = N_m \bar{m}^{\text{Water}} = 2.992 \times 10^{-26} N_m \text{ kg}. \quad (16)$$

Regarding the reference velocity, Kumar [30] used the average velocity in his Poiseuille flow model. In this paper, the thermal velocity will be used, so one can write

$$\bar{v}_{\text{ref}} = \sqrt{\frac{\bar{k}_B \bar{T}_{\text{ref}}}{\bar{m}_{\text{ref}}}} = 2.148 \times 10^1 \sqrt{\frac{\bar{T}_{\text{ref}}}{N_m}} \text{ m/s}. \quad (17)$$

As a result, the time reference can be derived as

$$\bar{t}_{\text{ref}} = \frac{\bar{r}_{\text{ref}}}{\bar{v}_{\text{ref}}} = 4.655 \times 10^{-2} \bar{r}_{\text{ref}} \sqrt{\frac{N_m}{\bar{T}_{\text{ref}}}} \text{ s}. \quad (18)$$

With all the above information, one can convert any dimensional parameter into the DPD units by following Eq. (19):

$$\begin{aligned} r &= \frac{\bar{r}}{\bar{r}_{\text{ref}}}, & m &= \frac{\bar{m}}{\bar{m}_{\text{ref}}}, & t &= \frac{\bar{t}}{\bar{t}_{\text{ref}}}, \\ v &= \frac{\bar{v}}{\bar{v}_{\text{ref}}}, & T &= \frac{\bar{T}}{\bar{T}_{\text{ref}}}, & e &= \frac{\bar{e}}{\bar{e}_{\text{ref}}}. \end{aligned} \quad (19)$$

In summary, only three inputs are needed to establish the unit references. Kumar [30] defines  $N_m$  first, whereas in this study,  $n_{\text{DPD}}$ ,  $\bar{r}_{\text{ref}}$ , and  $\bar{T}_{\text{ref}}$  will be chosen as the basis to derive the rest of unit references. Table I shows an example of the unit mapping when  $n_{\text{DPD}} = 4$ ,  $\bar{r}_{\text{ref}} = 1.0 \times 10^{-6} \text{ m}$ , and  $\bar{T}_{\text{ref}} = 300 \text{ K}$ . Therefore, from Eq. (5), one obtains  $a^{\text{Water-Water}} = 18.75$ .

### C. Simulation model

The sedimentation of a single Al particle in water will be studied under the length scale as  $\bar{r}_{\text{ref}} = 1 \mu\text{m}$  and the system temperature is set at room temperature so that  $\bar{T}_{\text{ref}} = 300 \text{ K}$  through the entire study.

A simulation box is created and filled with water particles of number density  $n_{\text{DPD}} = 4, 5, 6, 7, 8, 9$ , or 10. Periodic boundary conditions (PBCs) are applied along all directions. The system is first run under the constant number of particles, volume, and energy (NVE) ensemble for 1 000 steps so that the system will reach the thermal equilibrium status. In the second stage, the Al particle is placed at the top of the simulation box with a gravity added to it in  $z$  direction and simulation runs for another 100 000 steps. The DPD model can be found in Fig. 2(a).

However, this model has an inherent issue that the net force of the system is nonzero, which may keep accelerating the system if simulation is running long enough and lead to numerical instability. By monitoring the temperature profile in a simulation 10 times as long as the original test plan, a temperature rise less than 1% is observed and is plotted in the

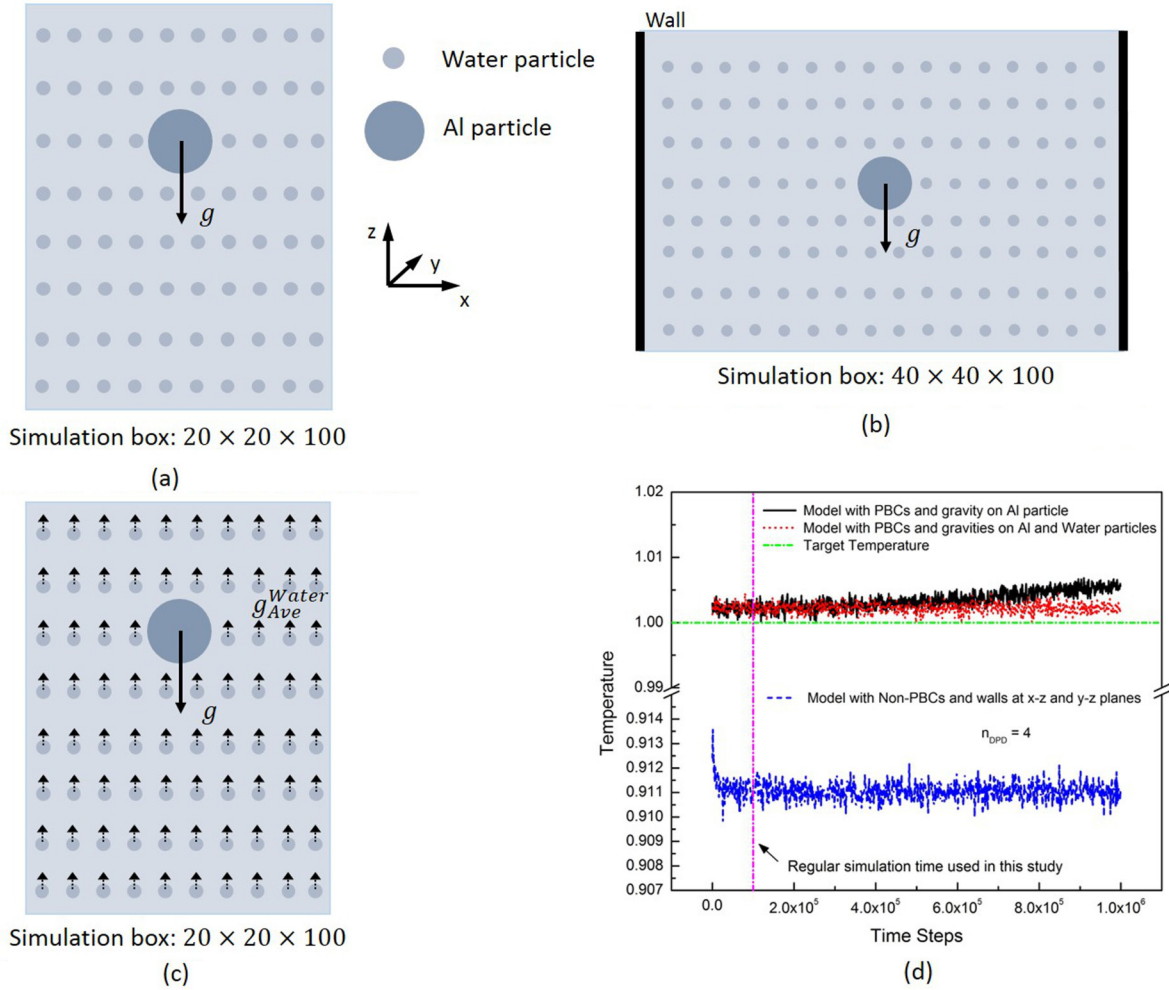


FIG. 2. (Color online) DPD models for particle sedimentation (a) with PBCs and gravity on Al particle; (b) with non-PBCs and walls at  $x$ - $z$  and  $y$ - $z$  planes; (c) with PBCs, gravity on Al particle, and opposite artificial force on water particles; and (d) comparison of the temperature profiles vs. simulation time steps among all models.

black solid line in Fig. 2(d). In order to fully understand this problem and further verify the model, two additional models have also been considered to balance the net force: the one with walls in  $x$ - $z$  and  $y$ - $z$  planes; and the other with PBCs, gravity on Al particle, and an opposite artificial force on water particles. The former balances the gravity force with the friction of wall and the latter balances the Al’s gravity by the artificial force on water particles.

In a real system, the steady state is achieved due to walls or boundary conditions imposed on the fluid at distances far from the settling particle. Based on this, a model, which is presented in Fig. 2(b), is built with walls in  $x$ - $z$  and  $y$ - $z$  planes, which are made of freezing DPD particles, and a bounce-back algorithm [16,18,57] is adopted here for particles moving outside of the wall. The PBC is only applied along  $z$  coordinate. However, this model requires a larger simulation domain since the Brownian motion may bring the Al particle too close to the wall. Although numerical details are not provided here, simulation results of the particle’s motion validate the model’s capability to repeat the Stokes’ flow at an infinite domain. While temperature rise is not observed, which is shown in blue dot line in Fig. 2(d), it is smaller than the target

temperature due to a substantial amount of inactive particles near the wall. By further enlarging the simulation box size, the equilibrium temperature certainly can approach to the target one, but the computation cost will be increased dramatically and the number of particles of the system easily exceeds the order of  $10^6$ .

While still applying PBCs along all directions, another model, which is shown in Fig. 2(c), has made a successful effort to overcome the nonzero net force deficiency. Since in a real system, the gravity is normally balanced by the external drag force on the liquid near the wall or the force from the bottom boundary. The magnitude of such drag force decreases as it moves further from the wall and reaches to zero eventually. One interesting idea to fix the nonzero net force issue while the computation cost is still affordable is to add an opposite artificial force on all water particles in the entire simulation domain, so that the total force exerted on the water particles and the Al particle can be balanced by using  $g_{Ave}^{Water} = m^{Al} g / (m^{Water} n_{DPD} V_{Vol})$ , where  $V_{Vol}$  is the volume of the simulation domain. If the simulation box is big enough (e.g., simulation box size is  $20 \times 20 \times 100$  and  $n_{DPD} = 4$ ),  $g_{Ave}^{Water}$  is in the order of  $10^{-5}$ . Numerical results of the temperature

profile, which is drawn in red dash line in Fig. 2(d), has verified our idea that the system is able to reach to the steady state where the equilibrium temperature is the target one and no temperature rise is observed for running a very long time simulation. Nonetheless, although the artificial force added on each individual water particle is small, there is a small decrease of the Al particle's terminal settling velocity from the Stokes' law. This is mainly due to the opposite artificial force added on water particles, which brings more resistance toward the Al particle's motion. Such discrepancy can be further reduced by increasing the simulation box, but the advantage in saving the computation cost will be lost again.

In summary, the net force issue in the present paper is caused by using a finite number of particles to simulate an infinitely large system. None of these three models can represent the Stokes' flow ideally. However, when the size of the simulation box increases, the difference of these models will decrease, which will converge to the Stokes' flow. Since the purpose of this paper is to establish a guide to show how to calibrate the DPD repulsive force parameter and the cut-off between solid-liquid particles, the Stokes flow of the infinite domain will be used to verify the models at an affordable computational cost without loss of the physics of particle motion. For the simple model with the nonzero net force, the results have shown that the particle reaches the terminal velocity very quickly, although the temperature of the system may rise 1% when running 10 times longer than the simulation length required in this study. This is mainly because the ratio of the mass of the Al particle over the total mass of water particles is a very small number and such local effect can be completely ignored from a global perspective. The two other alternative models introduce assumptions of the wall boundaries and the opposite artificial force on water particles, respectively, which address the net force issue very well. However, they have brought extra assumptions that do not necessarily help the simulation of the Stokes flow. Therefore, for parsimony of assumptions, the model with PBCs and gravity on the Al particle is used in this study although a nonzero net force of the system exists. However, notice that the system temperature may rise fast when the model size is small or the volume fraction of aluminum is considerable for a large particle system. Thereby, the two alternative models may serve as alternatives, which will be further studied in our future work.

#### D. Simulation plan

Compared with Groot and Warren's work [3], a smaller timestep ( $\Delta t = 0.005$ ) is chosen to ensure the numerical accuracy of the captured terminal settling velocity. It will be determined by the slope of Al particle's displacement along  $z$  coordinate from 50 000 timestep to the end of the simulation. In this way, a stable approximation of the terminal settling velocity can be obtained from the sample data with limited noise. Since the initial configuration of velocity profile of water particles and the DPD random force are related to some random seeds, which helps to generate random number of the Gaussian distribution, each test is run at least three times with different random seeds to get the average. Stokes' law is used to verify the terminal settling velocity by tuning the

repulsive force parameter  $a^{\text{Al-water}}$  and cut-off  $r_{\text{cut}}^{\text{Al-water}}$  between Al and water particles. The maximum  $a^{\text{Al-water}}$  in this study reaches to  $2 \times 10^4$ , which makes the potential essentially a hard core. If  $\Delta t$  is not small enough, the resulting particle trajectory for large  $a^{\text{Al-water}}$  may not be physical. In order to have consistent simulation parameters (timestep, duration, etc.),  $\Delta t = 0.005$  has been proven to serve a good balance between the numerical instability and reasonable time scale. Note that in a typical MD-like simulation, particle's neighbor list is built by scanning its surrounding particles within the distance of the force cutoff plus skin distance. In this study, even with a fixed timestep reduced to  $\Delta t = 0.005$  ( $\Delta t_{\text{max}} = 0.04$  for simulating pure water [3]), the skin distance may need to be slightly increased for a large  $a^{\text{Al-water}}$  (the default skin distance is 0.3 in DPD units). If the skin distance is increased too much compared with the force cutoff to construct a correct neighbor list, one may need to further reduce timestep to ensure the particle trajectory is physical and elongate the simulation to obtain meaningful averaged results.

The analytical expression of the Stokes' law is given as

$$V_{\text{Stokes}} = \frac{2}{9} \frac{(\rho^{\text{Al}} - n_{\text{DPD}})}{\mu_{\text{DPD}}} g (r^{\text{Al}})^2, \quad (20)$$

where  $\mu_{\text{DPD}}$  is the dynamic viscosity of DPD fluid calculated from Eq. (9).  $\mu_{\text{DPD}}$  can also be measured numerically by simulating periodic Poiseuille flow [23]. Through Marsh's [22] investigation of the viscosity using  $a^{\text{Water-Water}} = 0$ , one can see that it is accurate enough for a small  $a^{\text{Water-Water}}$ . Note that conventional DPD cannot obtain correct Schmidt number [ $Sc = \mu_{\text{DPD}} / (n_{\text{DPD}} D)$ ] and  $\bar{\mu}_{\text{DPD}}$  is also about several orders of magnitude smaller than  $\bar{\mu}_{\text{Water}}$  in physical units when  $\bar{r}_{\text{ref}} = 1 \mu\text{m}$ . However, based on the Stokes' law, the DPD system remains in the Stokes flow regime as long as the Reynolds number is less than one. The terminal settling velocity of the settling particle thereby can still be verified by the Stokes' law. Increasing  $\gamma^{\text{Water-Water}}$  [30] or modifying the DPD force terms [28,44,47] can match or approach the real viscosity, but it requires an extremely small  $\Delta t$ , which basically loses the timescale advantage of DPD. Because viscosity is indeed an outcome of DPD model and calibration of DPD parameters ( $a^{\text{Al-Water}}$  and  $r_{\text{cut}}^{\text{Al-Water}}$ ) is the main purpose of this parametric study, Eq. (5) and  $\gamma^{\text{Water-Water}} = 4.5$  from Groot and Warren's work [3] are used for all water-water particles interaction in this study.

Since the above Stokes' law occurs for single particle in the infinite domain at low Reynolds number, the dimension of the simulation box needs to be chosen carefully, in such a fashion that the boundary effect will not significantly change the Al particle's motion from the Stokes' law while the computational cost is still affordable. The effect of the simulation box's height is first examined, and a summary of the results is plotted in Fig. 3(a). Apparently, system temperature keeps increasing when the simulation box is only  $10 \times 10 \times 10$  in the DPD unit. This is caused by the images of the Al particle itself, which are brought by the periodic boundary conditions. As they keep heating the system, there is insufficient viscous force to balance the Al particle, which implies that the settling velocity of the Al particle is not able to achieve a stable value. After increasing the simulation box's height to 50, system temperature becomes stable. Although no obvious temperature increase is found, a slightly larger fluctuation around the target

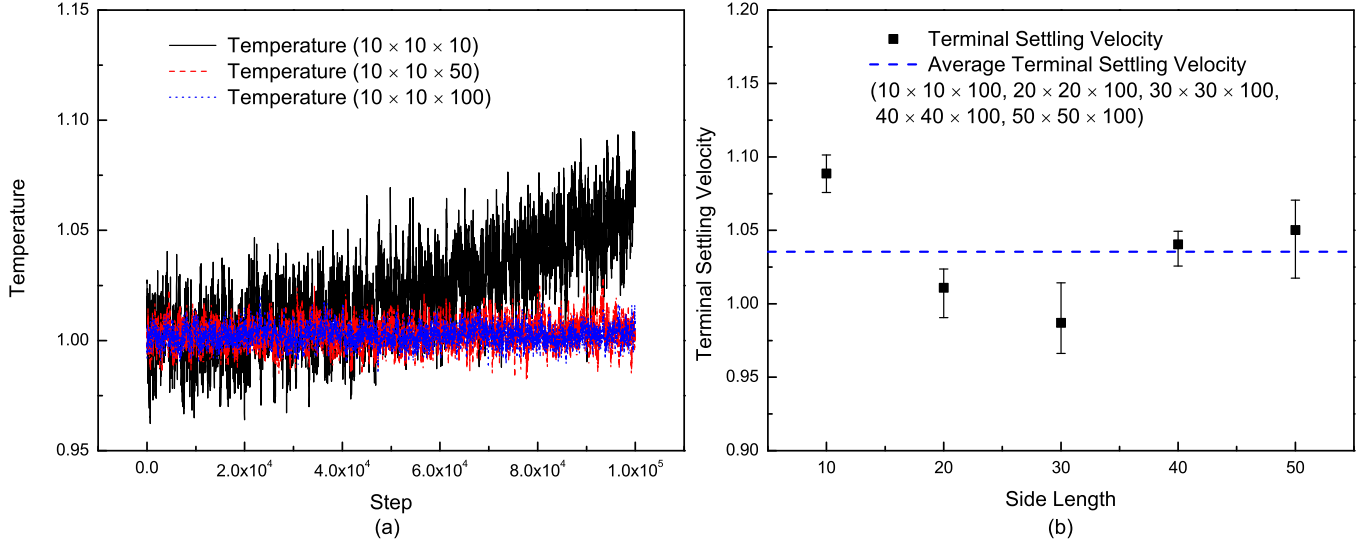


FIG. 3. (Color online) Comparison of different simulation box simulations. (a) Temperature profile at different simulation box heights:  $10 \times 10 \times 10$ ,  $10 \times 10 \times 50$ , and  $10 \times 10 \times 100$ ; (b) Terminal settling velocity of Al particle at different simulation box side length:  $10 \times 100$ ,  $20 \times 200$ ,  $30 \times 300$ ,  $40 \times 400$ , and  $50 \times 500$ .

temperature can be observed compared with the one when height is 100. Hence, 100 is selected for the simulation box height as a conservative choice. It is noted that this is only valid for a certain time interval, which has already been illustrated in Fig. 2(d). Additional computational experiments have been conducted to investigate the side length effect by increasing it from 10 to 50 with a fixed height at 100. The average of terminal settling velocities among all tests is used to measure whether the side length is large enough to produce an infinite domain for the Al particle and results are shown in the Fig. 3(b).

TABLE II. Simulation plan of the parametric study on particle sedimentation.

	Number Density $n_{\text{DPD}}$ Variation	
	In DPD scale	Mapped into physical scale
Case 1:		
$r^{\text{Al}}$	0.5	$0.5 \mu\text{m}$
$n_{\text{DPD}}$	4,5,6,7,8,9,10	$1.0 \times 10^3 \text{ kg/m}^3$
$g$	0.592	$9.810 \text{ m/s}^2$
$r_{\text{cut}}^{\text{Al-Water}}$	1.0	$1.0 \mu\text{m}$
$a^{\text{Al-Water}}$	$75k_B T/n_{\text{DPD}}, \dots, 2 \times 10^4$	
	Gravity $g$ Variation	
Case 2:		
$r^{\text{Al}}$	0.5	$0.5 \mu\text{m}$
$n_{\text{DPD}}$	4	$1.0 \times 10^3 \text{ kg/m}^3$
$g$	0.296, 0.148	$4.905, 2.453 \text{ m/s}^2$
$r_{\text{cut}}^{\text{Al-Water}}$	1.0	$1.0 \mu\text{m}$
$a^{\text{Al-Water}}$	$75k_B T/n_{\text{DPD}}, \dots, 10^4$	
	Radius $r^{\text{Al}}$ Variation	
Case 3:		
$r^{\text{Al}}$	0.25, 0.375, 0.75, 1.0	$0.25, 0.375, 0.75, 1.0 \mu\text{m}$
$n_{\text{DPD}}$	4	$1.0 \times 10^3 \text{ kg/m}^3$
$g$	$0.592 \times (r^{\text{Water}}/r^{\text{Al}})^3$	$9.810 \times (\bar{r}^{\text{Water}}/\bar{r}^{\text{Al}})^3 \text{ m/s}^2$
$r_{\text{cut}}^{\text{Al-Water}}$	0.5, ...2.0	$0.5, \dots 2.0 \mu\text{m}$
$a^{\text{Al-Water}}$	$75k_B T/n_{\text{DPD}}, \dots, 5 \times 10^4$	

When the side length is 10, the relative error is a little over 5%, while the rest of the tests have a relative error of less than 5%, which suggests  $20 \times 20 \times 100$  could be the best choice for the simulation box's dimension to mimic the infinite domain criteria, whereas the computation cost is still acceptable.

For the rest of this study, all simulations adopt  $20 \times 20 \times 100$  as the simulation box's dimension and a summary of the simulation plan is provided in the Table II. The number density will be varied in the first case and with each number density,  $a^{\text{Al-Water}}$  will be increased from  $a^{\text{Water-Water}}$  up to  $2 \times 10^4$ . For the second case, the gravity effect is examined while the radii effect is analyzed in the third case. Notice that any parameter without a particular unit indicates that it is in a reduced unit.

A C++ software package, named as particle dynamics parallel simulator (PDPS), is developed to fulfill this study. Message passing interface (MPI) is used here to manage the parallel computing and communications among processors based on spatial-decomposition algorithm [58]. It has been designed to focus on discrete particle methods at the mesoscopic level. For most of the simulations in this study, 16 processors are normally used for a single test and the simulation times varies from 2 to 24 h.

### III. RESULTS AND DISCUSSION

The goal of this work is to investigate the sedimentation of a particle moving in water and therefore provide a baseline for simulation of the sedimentation of a large particle system. In this paper, a single Al particle moving in water is considered. To accurately describe the motion of particles, following previous studies [30,46,47,59], the terminal velocity of the Al particle and the radial distribution function of water particles will be used for model verification with the Stokes flow formulation and particle distribution. However, this coarse-grain model will surely miss some information about the physics of fluid, for example, Schmidt's number ( $Sc = \nu/D$ ), viscosity ( $\nu$ ), or dimensionless compressibility, etc. [28,30,56].

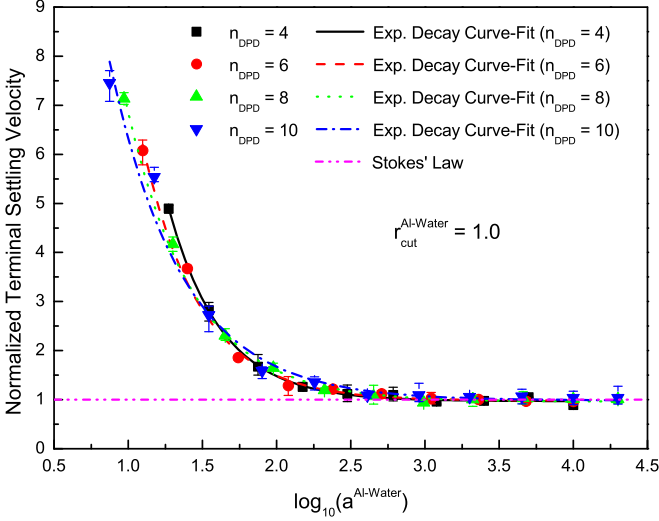


FIG. 4. (Color online) Normalized terminal settling velocity  $V_{\text{DPD}}^N$  of Al particle against  $\log_{10} a^{\text{Al-Water}}$  when  $n_{\text{DPD}} = 4, 6, 8, 10$ .

### A. Number density $n_{\text{DPD}}$ variation

Although DPD particles are essentially mathematical points, the occurrence of the interaction of two DPD particles with the same type can be presumed as two spheres with the same radius begin to contact with each other for consistent hydrodynamic behavior. Since the cutoff for water-water particles ( $r_{\text{cut}}^{\text{Water-Water}}$ ) is fixed to 1.0 as the reference length in DPD, water particle can be considered as a sphere with radius  $r^{\text{Water}} = 0.5$ . In this section, the radius of Al particle will also be fixed as 0.5, which implements that the cutoff  $r_{\text{cut}}^{\text{Al-Water}}$  is the same as  $r_{\text{cut}}^{\text{Water-Water}}$ .

For the case  $n_{\text{DPD}} = 4, 6, 8, 10$ , the terminal settling velocities are normalized by the corresponding  $V_{\text{Stokes}}$  from Stokes' law and plotted against  $\log_{10}(a^{\text{Al-Water}})$  in Fig. 4. Apparently, the terminal settling velocity decreases at the beginning and then becomes relatively stable and convergent to the Stokes' law for larger  $a^{\text{Al-Water}}$ . Results from other cases ( $n_{\text{DPD}} = 5, 7, 9$ ) follow the same observation described below. Surprisingly, all groups of points can be fit very well by the following exponential decay equation

$$V_{\text{DPD}}^N = A_1 e^{-\frac{\log_{10}(a^{\text{Al-Water}})}{t_1}} + V_{\text{DPD}}^{N-0}, \quad (21)$$

$$V_{\text{DPD}} = V_{\text{DPD}}^N V_{\text{Stokes}}, \quad (22)$$

$$V_{\text{DPD}}^0 = V_{\text{DPD}}^{N-0} V_{\text{Stokes}}, \quad (23)$$

where  $V_{\text{DPD}}^N$  is the normalized terminal settling velocity in DPD and the terms  $A_1$ ,  $t_1$ , and  $V_{\text{DPD}}^{N-0}$  are the three fitting coefficients. Obviously, from all groups, the normalized term  $V_{\text{DPD}}^{N-0}$  converges to 1.0, which indicates that  $V_{\text{DPD}}^0$  is actually the exact solution from the Stokes' law ( $V_{\text{Stokes}}$ ). The maximum error between  $V_{\text{DPD}}^0$  and  $V_{\text{Stokes}}$  is within 6%. It is also noticed that when  $a^{\text{Al-Water}}$  is relatively large, results will converge. This can also be explained by the fact that when  $a^{\text{Al-Water}}$  is large enough, the first term in the exponential decay equation

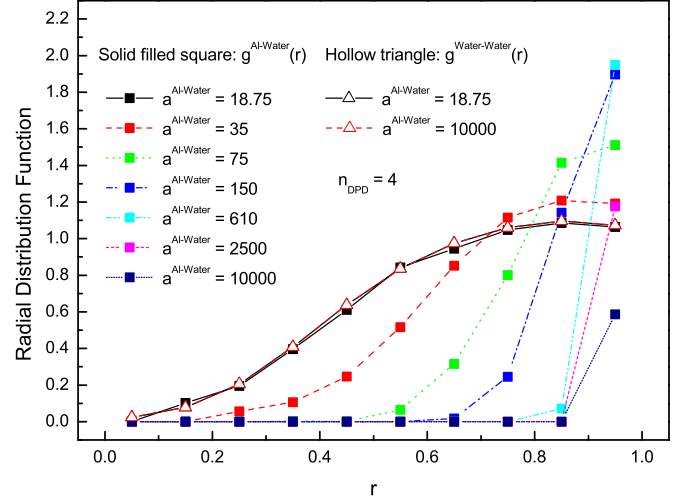


FIG. 5. (Color online) Al-water and water-water particles' radial distribution function profiles  $g^{\text{Al-Water}}(r)$  and  $g^{\text{Water-Water}}(r)$  with different  $a^{\text{Al-Water}}$  when  $n_{\text{DPD}} = 4$ .  $g^{\text{Al-Water}}(r)$ , solid filled square;  $g^{\text{Water-Water}}(r)$ , hollow triangle.

[Eq. (21)] vanishes and the second term  $V_{\text{DPD}}^{N-0}$  will make the result converge to the Stokes' law.

In order to reveal the physics lying behind this observation, Al-water and water-water particles' radial distribution functions  $g^{\text{Al-Water}}(r)$  and  $g^{\text{Water-Water}}(r)$ , which both describe the variation of water particles' local density as a function of Al and water particles' radius, respectively, are computed by scanning its surrounding water particle distribution at each time step and then averaging them over the last 50 000 steps. Results within the range of cutoff with different  $a^{\text{Al-Water}}$  are plotted in Fig. 5, where all Al-water particle's  $g^{\text{Al-Water}}(r)$  are represented by solid filled square shape and water-water particle's  $g^{\text{Water-Water}}(r)$  are represented by hollow triangle shape. When  $a^{\text{Al-Water}} = a^{\text{Water-Water}} = 18.75$ , the radial distribution profiles within the cutoff for Al-water and water-water particles are very similar. The small difference is caused by the gravity added on the Al particle only. As  $a^{\text{Al-Water}}$  increases, a larger repulsive force  $f_c$  between Al and water particles is obtained and thus  $g^{\text{Al-Water}}(r)$  decreases. The trend shown in Fig. 5 has implied that water particles are driven far from the Al particle. On the contrary,  $g^{\text{Water-Water}}(r)$  does not change with  $a^{\text{Al-Water}}$  due to the fact that water particles' motion is mainly determined by  $a^{\text{Water-Water}}$ , which is calculated from Eq. (5) as a constant. In reality, fluid particles should not penetrate into the solid particle and thus the solid particle can be treated as a rigid body when these two types of particles collide, whereas the fluid particles can deform freely. However, when  $a^{\text{Al-Water}}$  is small, the radial distribution function of Al particle at  $r \leq r^{\text{Al}} = 0.5$  in Fig. 5 is positive, which means the penetration of water particles. When  $a^{\text{Al-Water}}$  reaches 75 or higher,  $g^{\text{Al-Water}}(r \leq r^{\text{Al}})$  may reach zero.

However, although  $g^{\text{Al-Water}}(r \leq r^{\text{Al}})$  may reach zero at  $r = 0.5$  by increasing  $a^{\text{Al-Water}}$ , it does not guarantee a correct hydrodynamic interaction during the collision of Al and water particles. This explains why the terminal settling velocity of the Al particle is different from the Stokes' law, even though  $g^{\text{Al-Water}}(r \leq r^{\text{Al}})$  is very close to zero when  $a^{\text{Al-Water}} = 75$ .



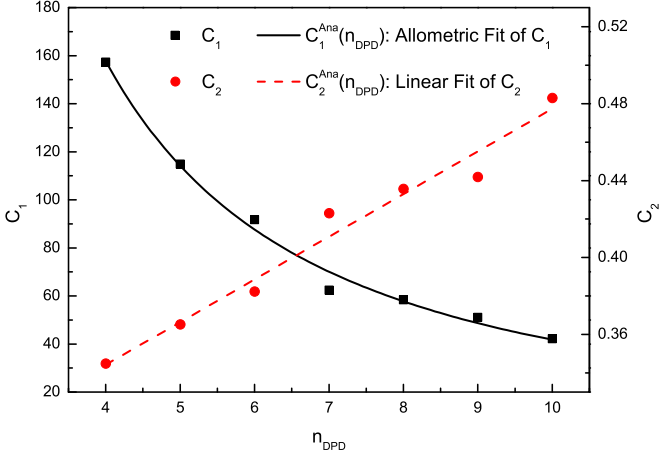


FIG. 6. (Color online) Curve-fit of coefficients  $C_1$  and  $C_2$  from Eq. (24) against  $n_{\text{DPD}}$ .

From the numerical experiments with  $n_{\text{DPD}} = 4$ , the minimum  $a^{\text{Water-Water}}$  should be around 610, which indicates that the threshold for the distance between the Al and water particles should locate at about 0.75, according to Fig. 5. By increasing  $a^{\text{Al-Water}}$  over a certain value,  $g^{\text{Al-Water}}(r)$  will become zero in most ranges of  $r \leq r_{\text{cut}}^{\text{Al-Water}}$ , which suggests water particles hardly fall into the Al particle's force interaction range. Therefore, continuously increasing  $a^{\text{Al-Water}}$  will no longer have a significant effect on the total conservative force  $\sum f_c$  on the settling Al particle, since the Al particle only interacts with water particles within the cutoff range. As a result, the relationship between the terminal settling velocity and  $\log_{10}(a^{\text{Al-Water}})$  exhibits an exponentially decaying characteristic. Compared with the rough sphere model [7,46,47], where a solid particle is constructed by a certain number of local freezing DPD fluid particles, only a single DPD particle with higher repulsive force parameter between the surrounding DPD fluid particles and itself is needed to represent the solid particle. Hence, the proposed DPD model in this study can be indeed considered as a simplified rough sphere model, which has already been verified by the Stokes' law.

Based on the theory proposed above, a modified exponential decay equation,

$$V_{\text{DPD}}^N = C_1 e^{\left[-\frac{\log_{10}(a^{\text{Al-Water}})}{C_2}\right]} + 1.0, \quad (24)$$

can be used to fit simulation results again, which yield two fitting coefficients  $C_1$  and  $C_2$ , and by doing allometric and linear fitting of them in Fig. 6, respectively, one can obtain the corresponding analytical functions  $C_1^{\text{Ana}}(n_{\text{DPD}})$  and  $C_2^{\text{Ana}}(n_{\text{DPD}})$  in terms of  $n_{\text{DPD}}$ , which are given by

$$C_1^{\text{Ana}}(n_{\text{DPD}}) = 1178.460 n_{\text{DPD}}^{-1.450}, \quad (25)$$

$$C_2^{\text{Ana}}(n_{\text{DPD}}) = 0.0222 n_{\text{DPD}} + 0.255. \quad (26)$$

Therefore, a universal empirical analytical expression for the normalized terminal settling velocity and nonnormalized one

TABLE III. Minimum value of  $a^{\text{Al-Water}}$  that describes the hydrodynamic interaction between Al and water particles when  $n_{\text{DPD}} = 4$  to 10.

$n_{\text{DPD}}$	4	5	6	7	8	9	10
$a_{\text{min}}^{\text{Al-Water}}$	593.19	681.53	798.77	947.10	1130.82	1355.78	1629.31

in DPD can be written as

$$V_{\text{DPD}}^{\text{N-Ana}} = C_1^{\text{Ana}}(n_{\text{DPD}}) e^{\left[-\frac{\log_{10}(a^{\text{Al-Water}})}{C_2^{\text{Ana}}(n_{\text{DPD}})}\right]} + 1.0 \quad (27)$$

$$V_{\text{DPD}}^{\text{Ana}} = V_{\text{DPD}}^{\text{N-Ana}} V_{\text{Stokes}} \quad (28)$$

From Eqs. (24) and (27), if  $a^{\text{Al-Water}}$  is chosen sufficiently large, the terminal settling velocity  $V_{\text{DPD}}$  should always converge to  $V_{\text{Stokes}}$ . However, this is not true in the actual DPD simulation. When  $a^{\text{Al-Water}}$  gets too large, there is only a fully elastic collision between Al and water particles. In reality, a small deformation of a water particle should be allowed since the water particle is much softer than the Al particle. Therefore, the largest value of  $a^{\text{Al-Water}}$  in this parametric study should be carefully determined in order to capture an exponentially decaying curve-fit and avoid numerical difficulties in the simulation. In this section,  $a_{\text{max}}^{\text{Al-Water}}$  is chosen to be  $10^4$  when  $n_{\text{DPD}} = 4, 5, 6, 7$  and  $2 \times 10^4$  when  $n_{\text{DPD}} = 8, 9, 10$ , respectively. Thereby, it is also necessary to define the minimum  $a^{\text{Al-Water}}$  as a threshold to match  $V_{\text{DPD}}^{\text{Ana}}$  from Eq. (28) to the Stokes' law  $V_{\text{Stokes}}$  while maintaining acceptable numerical accuracy. In this study, we use 3% as the relative error between DPD and Stokes' law results and minimum  $a^{\text{Al-Water}}$  can be then derived from Eq. (27) as

$$\begin{aligned} a_{\text{min}}^{\text{Al-Water}} &= 10^{-C_2^{\text{Ana}} \ln[0.03/C_1^{\text{Ana}}]} \\ &= 10^{-(0.0222n_{\text{DPD}}+0.255) \ln[0.03/(1178.460n_{\text{DPD}}^{-1.450})]}. \end{aligned} \quad (29)$$

The exact numerical values are presented in the Table III as an reference. Apparently,  $a_{\text{min}}^{\text{Al-Water}}$  becomes larger as  $n_{\text{DPD}}$  increases. This is due to the fact that as  $n_{\text{DPD}}$  raises,  $N_m$  from Eq. (15) will decrease resulting in a decrease of the mass reference provided in Eq. (16). Based on the Eq. (19), mass of Al particle  $m^{\text{Al}}$  will thereby decrease since the the mass of Al particle  $\bar{m}^{\text{Al}}$  is a constant value in the physical unit. As the Al particle in the DPD scale becomes "heavier," the Al-water particle interaction needs more strength to be balanced during the settling and to achieve the Stokes' law eventually.

## B. Gravity $g$ variation

From the Stokes' law [Eq. (20)], the terminal settling velocity has a linear relationship with the gravity. To test whether this criteria holds in DPD, two additional gravities are also considered in the following. All other parameters are still the same from the last section. Applying the exponential decay curve fit Eq. (21), the normalized terminal settling velocities for  $g = 0.592, 0.296, 0.148$  are presented in Fig. 7. Apparently, all curves eventually lie on the horizontal curve ( $y = 1.0$ ), which confirms the theory made in the last section,

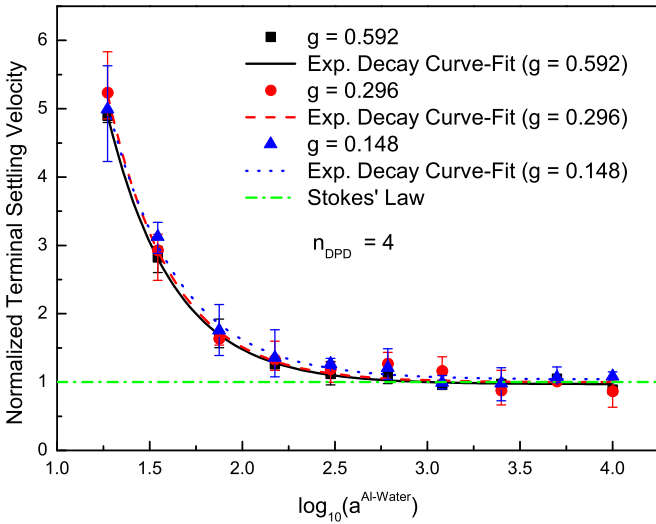


FIG. 7. (Color online) Normalized terminal settling velocity  $V_{DPD}^N$  of Al particle against  $\log_{10} a^{Al-Water}$  when  $g = 0.592, 0.296, 0.148$ .

and it also can be seen that the effect of gravity on the shape of the curve can almost be ignored. Comparison between the term  $V_{DPD}^0$  from Eq. (23) and Stokes' law ( $V_{Stokes}$ ) is shown in Fig. 8. Obviously, a linear relation between the terminal settling velocity and gravity is also observed, which shows excellent agreement between the DPD and Stokes' law.

Notice that the Stokes' law is only valid for a flow with Reynolds number less than one. This is also true in DPD where the Reynolds number is calculated as  $2V_{DPD}r^{Al}/\nu_{DPD}$ . If it is too large, DPD fluid cannot provide sufficient drag force for the settling particle to reach its terminal settling velocity. In addition, if the Reynolds number is too small, a large fluctuation due to the numerical error may appear. This is because if the terminal settling velocity is a very small number, which means the mapped one in the physical units is much smaller than the thermal velocity from Eq. (17), the settling of the Al particle will be interrupted intensively by the relatively strong Brownian motion. One may need

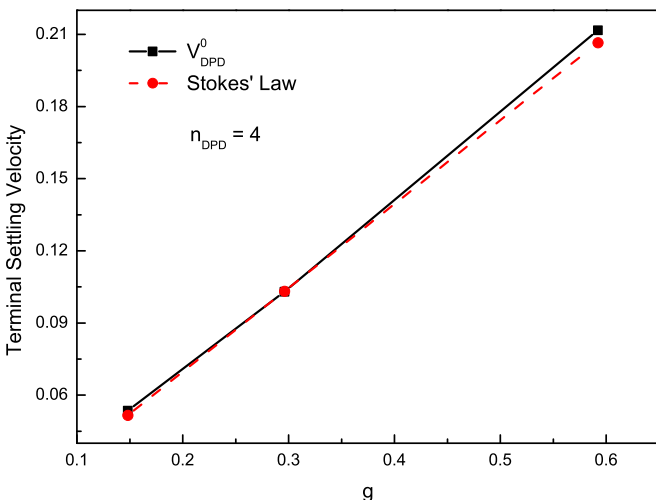


FIG. 8. (Color online) Term  $V_{DPD}^0$  of Eq. (23) against gravity  $g$ .

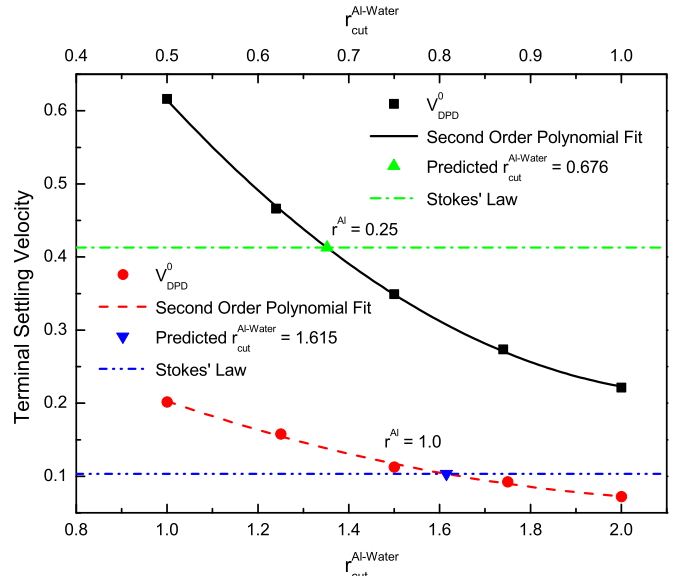


FIG. 9. (Color online) Term  $V_{DPD}^0$  of Eq. (23) against  $r^{Al-Water}_{cut}$  when  $r^{Al} = 0.25, 1.0$ .

to extend the simulation duration substantially to extract an accurate terminal settling velocity of the Al particle. In the following, Reynolds numbers are computed as 0.76, 0.38, and 0.19, corresponding to the gravity 0.592, 0.296, and 0.148, respectively. Simulation for the case  $g = 0.148$  takes  $2 \times 10^5$  steps particularly to prevent large numerical fluctuation.

### C. Radius $r^{Al}$ variation

In this section, different radii of Al particles will be considered. In order to maintain the Reynolds number when  $r^{Al} = 0.5$ ,  $n_{DPD} = 4$ , and  $g = 0.592$  in the first group of tests (of Fig. 4), gravity  $g = 0.592$  is multiplied with the factor  $(r^{Water}/r^{Al})^3$  correspondingly to each test.

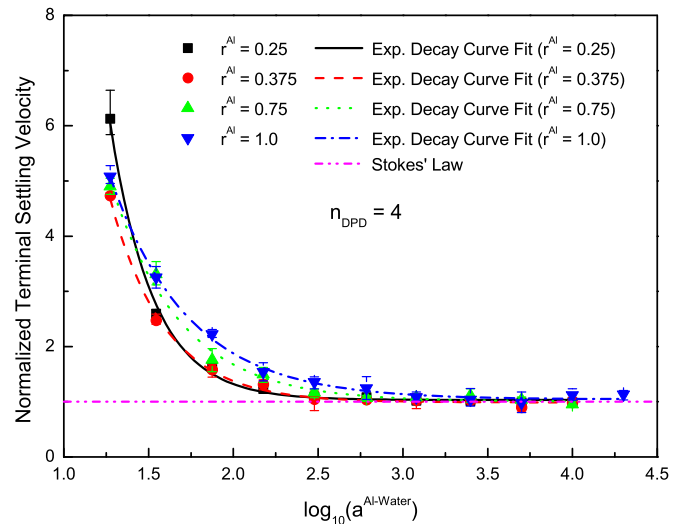


FIG. 10. (Color online) Normalized terminal settling velocity  $V_{DPD}^N$  of the Al particle against  $\log_{10} a^{Al-Water}$  when  $r^{Al} = 0.25, 0.375, 0.75, 1.0$ .

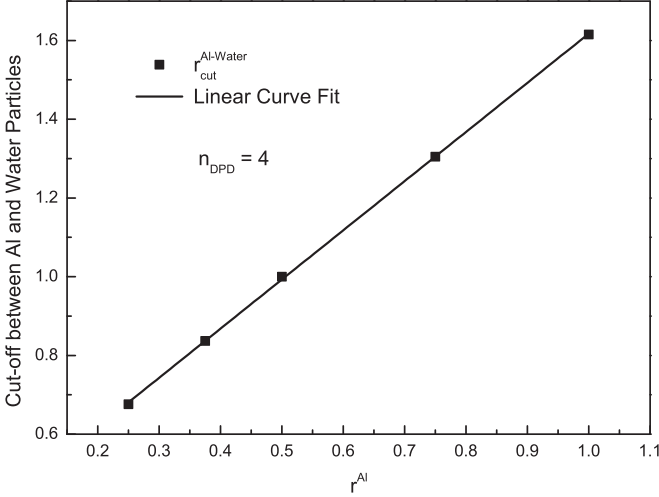


FIG. 11. Predicted cut-off  $r_{\text{cut}}^{\text{Al-Water}}$  against radius  $r^{\text{Al}}$ .

The radius of the Al particle will be first decreased to  $r^{\text{Al}} = 0.25$ . By using the same cutoff that  $r_{\text{cut}}^{\text{Al-Water}} = r_{\text{cut}}^{\text{Water-Water}} = 1.0$ , the term  $V_{\text{DPD}}^0$  from Eq. (23) is found to be lower than the Stokes' law. Since the radius of Al particle is decreased, the Al-Water particles' cut-off  $r_{\text{cut}}^{\text{Al-Water}}$  may also need to be decreased so that less number of water particles will interact with the Al particle, which means a less viscous force will be exerted on it. An opposite phenomenon is observed when  $r^{\text{Al}}$  is increased to 1.0, which suggests increasing the cutoff between Al and water particles so that more viscous force is able to decrease the terminal settling velocity. By testing different  $r_{\text{cut}}^{\text{Al-Water}}$  for each case, all results are presented in Fig. 9. A second-order polynomial is assumed for the relation between the term  $V_{\text{DPD}}^0$  and  $r_{\text{cut}}^{\text{Al-Water}}$ , which is also inspired from the Stokes' law [Eq. (20)], where the terminal settling velocity has the same relation with the particle's radius. The interception of the second-order polynomial curve-fit and Stokes' law yields the predicted Al and water particles' cut-off as  $r_{\text{cut}}^{\text{Al-Water}} = 0.676, 1.615$  for  $r^{\text{Al}} = 0.25, 1.0$ , respectively. By following the same procedure, one can find the cutoff  $r_{\text{cut}}^{\text{Al-Water}} = 0.837$  and  $1.305$  for  $r_{\text{cut}} = 0.375$  and  $0.75$ , respectively. Adopting these

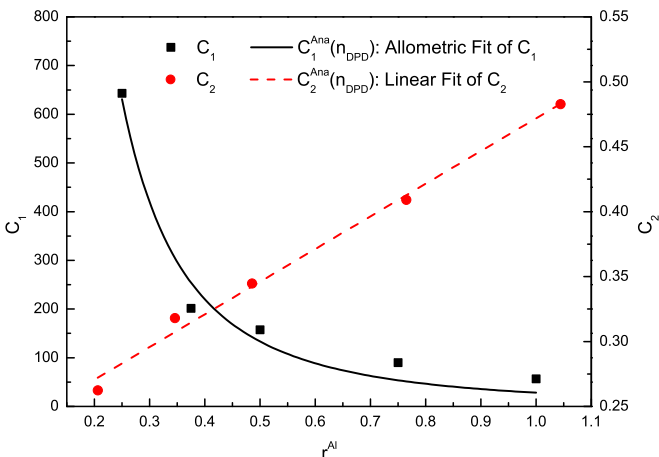


FIG. 12. (Color online) Curve-fit of coefficients  $C_1$  and  $C_2$  from Eq. (24) against radius  $r^{\text{Al}}$ .

TABLE IV. Minimum value of  $a^{\text{Al-Water}}$  that describes hydrodynamic interaction between Al and water particles when  $r^{\text{Al}} = 0.25, 0.375, 0.50, 0.75, 1.0$  and  $n_{\text{DPD}} = 4$ .

$r^{\text{Al}}$	0.250	0.375	0.500	0.750	1.000
$a_{\text{min}}^{\text{Al-Water}}$	593.19	602.68	753.14	1235.20	2025.00

predicted cutoffs, additional DPD simulations are carried out, and the results have shown the convergence to the Stokes' law in Fig. 10.

Combing all the results above, the predicted  $r_{\text{cut}}^{\text{Al-Water}}$  with respect to the radius of the Al particle  $r^{\text{Al}}$  is shown in Fig. 11. Apparently, a linear relationship is observed and an approximation for the correct cutoff is given by

$$r_{\text{cut}}^{\text{Al-Water}} = 1.249r^{\text{Al}} + 0.369. \quad (30)$$

To determine the minimum repulsive force parameter between Al and water particles, say  $a_{\text{min}}^{\text{Al-Water}}$  in terms of  $r^{\text{Al}}$ , a curve-fitting should be conducted to calculate  $C_1$  and  $C_2$  for Eq. (24) at different values of  $r^{\text{Al}}$ . For example, Fig. 12 illustrates the values of  $C_1$  and  $C_2$  for  $n_{\text{DPD}} = 4$  versus  $r^{\text{Al}}$  in the range of 0.25 to 1.0, in which  $C_1$  exhibits an allometric trend and  $C_2$  exhibits a linear trend. Therefore,  $C_1$  and  $C_2$  can be explicitly written in terms of the corresponding functions. Then, through Eq. (24) with the same threshold 3% as adopted in Eq. (29),  $a_{\text{min}}^{\text{Al-Water}}$  can be expressed as

$$\begin{aligned} a_{\text{min}}^{\text{Al-Water}} &= 10^{-C_2^{\text{Ana}}[\ln(0.03/C_1^{\text{Ana}})]} \\ &= 10^{-(0.281r^{\text{Al}}+0.202)\ln[0.03/(28.192(r^{\text{Al}})^{-2.242})]}. \end{aligned} \quad (31)$$

Its numerical values at different values of  $r^{\text{Al}}$  are presented in Table. IV. Notice that although  $a_{\text{min}}^{\text{Al-Water}}$  is larger than the one in Table III when  $r^{\text{Al}} = 0.5$ , they are in the same magnitude and such small discrepancy will not make any significant effect on the simulation results. Hence, one can choose the larger one as a conservative choice.

#### IV. CONCLUSION

A simplified rough sphere model, which uses a single DPD bead to represent the solid particle, is proposed to simulate particle sedimentation in a DPD fluid. A systematic parametric study on the repulsive force parameter and cut-off between Al and water particles has been presented for varying sizes of Al particles. The terminal settling velocities against  $\log_{10}(a^{\text{Al-Water}})$  can be well fit by the exponential decay equation [Eq. (21)], where the term  $V_{\text{DPD}}^{N-0}$  actually indicates the one from Stokes' law. Therefore, when the repulsive force parameter  $a^{\text{Al-Water}}$  is above a certain value, the terminal settling velocity will approach to the Stokes' law and an analytical expression of the  $a_{\text{min}}^{\text{Al-Water}}$  as a function of the number density  $n_{\text{DPD}}$  is also provided in Eq. (29). Radial distribution functions  $g^{\text{Al-Water}}(r)$  and  $g^{\text{Water-Water}}(r)$  of Al-water and water-water particles, respectively, are presented to reveal the fundamental physics lying behind this observation. It has been illustrated that  $a^{\text{Al-Water}}$  needs to be chosen above a certain threshold to avoid nonphysical collision of Al and water particles. The

profile of  $g^{\text{Al-Water}}(r)$  corresponding to the  $a_{\text{min}}^{\text{Al-Water}}$  has actually reflected the small deformation of water particle during the collision. Moreover, the existence of the linear relationship between the terminal settling velocity and gravity has also been demonstrated. Another linear relationship is also observed between the desirable cutoff  $r_{\text{cut}}^{\text{Al-Water}}$  and  $r^{\text{Al}}$ . Two analytical empirical equations are derived to guide researchers to choose  $r_{\text{cut}}^{\text{Al-Water}}$  [Eq. (30)] and  $a_{\text{min}}^{\text{Al-Water}}$  [Eq. (31)] in terms of  $r^{\text{Al}}$ .

By following a similar procedure, an empirical equation could be derived to find correct hydrodynamic behavior between any type of solid and liquid particles in DPD. Moreover, it is also important and necessary to further improve the DPD model to overcome the difficulties in the coarse-

graining process by matching the Schmidt's number, viscosity, and dimensionless compressibility, etc., of a real fluid.

#### ACKNOWLEDGMENTS

The authors thank Dr. Po-Hua Lee, Mr. Mostafa Mobasher, and Mr. Yingjie Liu for their valuable assistance and discussion. This work is also sponsored by the National Science Foundation (Grants No. CMMI 0954717, No. CMMI 1301288, and No. CMMI 1301160), whose support is gratefully acknowledged. In addition, Yin appreciates the support of the Henry Mitchell Weitzner Research Fund, for his research of materials for solar energy applications and technologies.

- 
- [1] G. K. Batchelor, *An Introduction to Fluid Dynamics* (Cambridge University Press, Cambridge, 2000).
- [2] D. C. Rapaport, *The Art of Molecular Dynamics Simulation* (Cambridge University Press, Cambridge, UK/New York, NY, 2004).
- [3] R. D. Groot and P. B. Warren, *J. Chem. Phys.* **107**, 4423 (1997).
- [4] E. Moendarbary, T. Y. Ng, and M. Zangeneh, *Int. J. Appl. Mech.* **01**, 737 (2009).
- [5] P. J. Hoogerbrugge and J. M. V. A. Koelman, *Europhys. Lett.* **19**, 155 (1992).
- [6] J. M. V. A. Koelman and P. J. Hoogerbrugge, *Europhys. Lett.* **21**, 363 (1993).
- [7] E. S. Boek, P. V. Coveney, H. N. W. Lekkerkerker, and P. van der Schoot, *Phys. Rev. E* **55**, 3124 (1997).
- [8] P. De Palma, P. Valentini, and M. Napolitano, *Phys. Fluids* **18**, 027103 (2006).
- [9] W. Pan, B. Caswell, and G. E. Karniadakis, *Langmuir* **26**, 133 (2010).
- [10] A. Maiti and S. McGrother, *J. Chem. Phys.* **120**, 1594 (2004).
- [11] W. Jiang, J. Huang, Y. Wang, and M. Laradji, *J. Chem. Phys.* **126**, 044901 (2007).
- [12] T. W. Sirk, Y. R. Slizoberg, J. K. Brennan, M. Lisal, and J. W. Andzelm, *J. Chem. Phys.* **136**, 134903 (2012).
- [13] D. Visser, H. Hoefsloot, and P. Iedema, *J. Comput. Phys.* **214**, 491 (2006).
- [14] P. Meakin and Z. Xu, *Progr. Comput. Fluid Dynam. Int. J.* **9**, 399 (2009).
- [15] S. M. Willemsen, H. C. J. Hoefsloot, and P. D. Iedema, *Int. J. Mod. Phys. C* **11**, 881 (2000).
- [16] D. Duong-Hong, N. Phan-Thien, and X. Fan, *Comput. Mech.* **35**, 24 (2004).
- [17] I. V. Pivkin and G. E. Karniadakis, *J. Comput. Phys.* **207**, 114 (2005).
- [18] I. V. Pivkin and G. E. Karniadakis, *Phys. Rev. Lett.* **96**, 206001 (2006).
- [19] P. B. Warren, *Phys. Rev. E* **68**, 066702 (2003).
- [20] M. Arienti, W. Pan, X. Li, and G. Karniadakis, *J. Chem. Phys.* **134**, 204114 (2011).
- [21] A. Ghoufi, J. Emile, and P. Malfreyt, *Eur. Phys. J. E* **36**, 10 (2013).
- [22] C. A. Marsh, G. Backx, and M. H. Ernst, *Phys. Rev. E* **56**, 1676 (1997).
- [23] J. A. Backer, C. P. Lowe, H. C. J. Hoefsloot, and P. D. Iedema, *J. Chem. Phys.* **122**, 154503 (2005).
- [24] G. Besold, I. Vattulainen, M. Karttunen, and J. M. Polson, *Phys. Rev. E* **62**, R7611 (2000).
- [25] I. Vattulainen, M. Karttunen, G. Besold, and J. M. Polson, *J. Chem. Phys.* **116**, 3967 (2002).
- [26] A. Chaudhri and J. R. Lukes, *Phys. Rev. E* **81**, 026707 (2010).
- [27] C. P. Lowe, *Europhys. Lett.* **47**, 145 (1999).
- [28] I. V. Pivkin and G. E. Karniadakis, *J. Chem. Phys.* **124**, 184101 (2006).
- [29] R. M. Fehslin, H. Fellermann, A. Eriksson, and H.-J. Ziock, *J. Chem. Phys.* **130**, 214102 (2009).
- [30] A. Kumar, Y. Asako, E. Abu-Nada, M. Krafczyk, and M. Faghri, *Microfluid. Nanofluid.* **7**, 467 (2009).
- [31] J. R. Spaeth, I. G. Kevrekidis, and A. Z. Panagiotopoulos, *J. Chem. Phys.* **134**, 164902 (2011).
- [32] J. R. Spaeth, T. Dale, I. G. Kevrekidis, and A. Z. Panagiotopoulos, *Ind. Eng. Chem. Res.* **50**, 69 (2011).
- [33] E. E. Keaveny, I. V. Pivkin, M. Maxey, and G. E. Karniadakis, *J. Chem. Phys.* **123**, 104107 (2005).
- [34] V. Symeonidis, G. E. Karniadakis, and B. Caswell, *J. Chem. Phys.* **125**, 184902 (2006).
- [35] D. Cubero and S. N. Yaliraki, *Phys. Rev. E* **72**, 032101 (2005).
- [36] D. Cubero, *J. Chem. Phys.* **128**, 147101 (2008).
- [37] R. D. Groot and K. L. Rabone, *Biophys. J.* **81**, 725 (2001).
- [38] J. C. Shillcock and R. Lipowsky, *J. Chem. Phys.* **117**, 5048 (2002).
- [39] J. R. Spaeth, I. G. Kevrekidis, and A. Z. Panagiotopoulos, *J. Chem. Phys.* **135**, 184903 (2011).
- [40] A. Ghoufi and P. Malfreyt, *Phys. Rev. E* **83**, 051601 (2011).
- [41] X. Yong, O. Kuksenok, K. Matyjaszewski, and A. C. Balazs, *Nano Lett.* **13**, 6269 (2013).
- [42] J. C. Shillcock and R. Lipowsky, *Nat. Mater.* **4**, 225 (2005).
- [43] A. A. Gavrilov, A. V. Chertovich, P. G. Khalatur, and A. R. Khokhlov, *Soft Matter* **9**, 4067 (2013).
- [44] X. Fan, N. Phan-Thien, S. Chen, X. Wu, and T. Yong Ng, *Phys. Fluids* **18**, 063102 (2006).
- [45] W. Pan, D. A. Fedosov, G. E. Karniadakis, and B. Caswell, *Phys. Rev. E* **78**, 046706 (2008).
- [46] J. M. Kim and R. J. Phillips, *Chem. Eng. Sci.* **59**, 4155 (2004).
- [47] S. Chen, N. Phan-Thien, B. C. Khoo, and X. J. Fan, *Phys. Fluids* **18**, 103605 (2006).

- [48] W. Pan and A. M. Tartakovsky, *Advances in Water Resources* **58**, 41 (2013).
- [49] D. J. Yang and H. M. Yin, *IEEE Trans. Energy Conv.* **26**, 662 (2011).
- [50] D. J. Yang, Z. F. Yuan, P.-H. Lee, and H. M. Yin, *Int. J. Heat Mass Transf.* **55**, 1076 (2012).
- [51] H. M. Yin, D. J. Yang, G. Kelly, and J. Garant, *Solar Energy* **87**, 184 (2013).
- [52] H. M. Yin, L. M. Li, P. Prieto-Munoz, and M. E. Lackey, “Functionally graded solar roofing panels and systems” (2012), U.S. Classification 136/248, 136/246; International Classification H01L31/058, H01L31/052; Cooperative Classification Y02E10/60, Y02E10/52, Y02B10/70, Y02B10/20, H01L31/058, Y02B10/12; European Classification H01L31/058.
- [53] P.-H. Lee and H. M. Yin, *J. Nanomech. Micromech.* A4014008.
- [54] Y. J. Liu and H. M. Yin, *Acta Mech.* **225**, 1429 (2014).
- [55] P. Espaol and P. Warren, *Europhys. Lett.* **30**, 191 (1995).
- [56] Z. Li and G. Drazer, *Phys. Fluids* **20**, 103601 (2008).
- [57] D. Visser, H. Hoefsloot, and P. Iedema, *J. Comput. Phys.* **205**, 626 (2005).
- [58] S. Plimpton, *J. Comput. Phys.* **117**, 1 (1995).
- [59] I. Pagonabarraga and D. Frenkel, *J. Chem. Phys.* **115**, 5015 (2001).